Limnol. Oceanogr., 57(2), 2012, 486–502

doi:10.4319/lo.2012.57.2.0486

Nutrient dynamics and biological consumption in a large continental shelf system under the influence of both a river plume and coastal upwelling

Aiqin Han,[a] Minhan Dai,[a,*] Shuh-Ji Kao,[a,b] Jianping Gan,[c,d] Qing Li,[a] Lifang Wang,[a] Weidong Zhai,[a] and Lei Wang[a]

[a] State Key Laboratory of Marine Environmental Science, Xiamen University, Xiamen
[b] Research Center of Environmental Changes, Academia Sinica, Taipei
[c] Department of Mathematics, Hong Kong University of Science and Technology, Kowloon, Hong Kong
[d] Division of Environment, Hong Kong University of Science and Technology, Kowloon, Hong Kong

Abstract

We examined the dynamics of dissolved inorganic nitrogen (DIN, nitrate + nitrite), dissolved inorganic phosphorus (DIP), and silicate ($Si(OH)_4$) in the northern shelf of the South China Sea in summer, which is under a complex hydrodynamic scheme largely shaped by river plume and coastal upwelling, along with the enhanced biological consumption of nutrients therein. The Pearl River plume, with high nutrient concentrations ($\sim$ 0.1–14.2 μmol L^{-1} for DIN, $\sim$ 0.02–0.10 μmol L^{-1} for DIP, and $\sim$ 0.2–18.9 μmol L^{-1} for $Si(OH)_4$), occupied a large area of the middle shelf (salinity $<$ 33.5). The nearshore area had high nutrient concentrations apparently sourced from subsurface nutrient-replete waters through wind-driven coastal upwelling. These nutrient levels were significantly elevated relative to those on the oligotrophic outer shelf where DIN, DIP, and $Si(OH)_4$ concentrations dropped to $<$ 0.1 μmol L^{-1}, $\sim$ 0.02–0.03 μmol L^{-1}, and $\sim$ 2.0 μmol L^{-1}, respectively. A three end-member mixing model was constructed based on potential temperature and salinity conservation to assess biological consumption of inorganic nutrients, which was denoted by Δ and defined by the deviation from conservative mixing. In the coastal upwelling zone and deep chlorophyll maximum layer, the nutrient uptake ratio $\Delta DIN : \Delta DIP$ was 16.7, which is the classic Redfield ratio. In contrast, in the river plume the uptake ratio was 61.3 $\pm$ 8.7. We believed that an alternative non-DIP source likely contributed to this higher DIN : DIP consumption ratio in the river plume regime. Meanwhile, $Si(OH)_4$ showed predominant consumption in the river plume and a combination of regeneration and consumption along the path of the coastal upwelling current.

River inputs and their responses in shelf ecosystems to the changing environment have received considerable attention during the past few decades (Dagg et al. 2008; Bianchi and Allison 2009; Cao et al. 2011). The motivation underlying such research is associated with the fact that riverine inputs of material are the primary source of nutrients sustaining shelf ecosystems. This is particularly true in large river–shelf systems where the river discharge dominates the shelf nutrient dynamics and thus the biological productivities (Chen 2008). Moreover, any changes in river inputs of nutrients and their composition can cause alterations of community structure downstream on the shelf. Such changes are likely under both the context of global climate changes and anthropogenic scenarios. Mechanistic and quantitative understanding of such inputs and their responses remains difficult, however, because of the highly variable plume dynamics and biological responses to the plume-derived nutrients (Lohrenz et al. 1999).

Another well-known and important nutrient source in many world shelf systems is coastal upwelling under favorable wind and topography conditions (van Geen et al. 2000; Gan et al. 2009*a*). Upwelling brings nutrient-replete water to the surface along the coast, and this may stimulate biological productivity and may also further complicate the nutrient dynamics in the shelf ecosystem. The intensity of wind-driven coastal upwelling, and thus the intensity of nutrient flux from depth, is governed not only by the strength of wind forcing, but also by characteristics of shelf topography. The variable upwelling along the coast largely affects the variability of biogeochemical processes.

River plume and coastal upwelling are interactive. The plume is transported by the upwelling circulation, while the buoyancy of the plume modulates the circulation over the shelf (Gan et al. 2009*b*). Although the riverine nutrient input tends to be a dominant source in many coastal waters, contributions from nutrient transport by upward ocean circulation also play a significant role. This adds more difficulties in elucidating the biogeochemical processes involved (Cao et al. 2011). Chen (1996) reports that upwelling-derived nutrients surpass river inputs from the Changjiang in the East China Sea shelf system. The relative importance of nutrients contributed from river plume and coastal upwelling, however, remains largely unclear in many river–shelf systems primarily due to complex physical and biological dynamics. Moreover, what remains unidentified in such complex systems is the biological response to differing composition in inorganic nutrients between the upwelled and plume waters. Typically, a river plume carries nutrient-enriched waters with a high dissolved inorganic nitrogen : dissolved inorganic phosphorus, or DIN : DIP ratio (Jickells 1998), whereas upwelling brings up waters from deeper layers with DIN : DIP resembling the Redfield ratio (Redfield et al. 1963; Chen et al. 2003). For example, in the East China Sea, massive riverine nutrient input has led to a large surface area having "excess nitrate," or being phosphorus limited (Chen 2008).

* Corresponding author: mdai@xmu.edu.cn

Evidence shows that the unbalanced nutrient composition might have caused an alteration of community structure and stimulated the growth of harmful algae (Varkitzi et al. 2010) and even influenced the amount of carbon sequestration, since the cellular C : P ratio of plankton varies concomitantly with DIN : DIP (Geider and Roche 2002).

In examining the nutrient dynamics in shelf systems, nutrient speciation and bioavailability are other issues to be considered. For example, it has long been debated whether dissolved organic phosphorus (DOP) is bioavailable (Karl and Björkman 2002). Growing evidence suggests that under conditions of DIP depletion, DOP may be stimulated to become bioavailable by the phytoplankton metabolized alkaline phosphatase enzyme activity (APA) (Nicholson et al. 2006). However, much remains unknown concerning the balance between DIP and DOP in river plume systems where DIP is commonly consumed by biological productivity along the path of the plume.

This study, based on a carefully designed process study cruise, set out to examine the nutrient dynamics and biological consumption in a complex physical and biogeochemical system modulated largely by both the river plume and coastal upwelling. By adopting a three end-member mixing model, we were able to semiquantitatively estimate the relative rates of consumption between DIN, DIP, and silicate ($Si(OH)_4$). We found that in different regions with differing nutrient input sources, the apparent uptake ratios of nutrients were different. The DIN : DIP uptake ratio in coastal upwelling regions and at the deep chlorophyll maximum (DCM) layer was almost identical to the canonical Redfield ratio but was anomalously as high as 61.3 ± 8.7 in the plume waters. Such apparent non-Redfield uptake ratio in the river plume suggested that a high N : P substrate might be produced or that non-DIP might be the important source. In addition, $Si(OH)_4$ appeared to be more dynamic, showing a much more complicated picture, with predominant consumption in the river plume and a combination of regeneration and consumption in the path of the coastal upwelling circulation. To our knowledge, this study was among the first attempt to pin down multinutrient uptake ratios using a combination of field observations and a simple three end-member mixing model in a complex shelf system under the influences of both a river plume and coastal upwelling. The insightful nutrient dynamics obtained in the study are important in defining the river–shelf ecosystem.

Methods

Site description—The Pearl River, as the primary freshwater source emptying into the Northern South China Sea (NSCS), is the world's 13th largest river in terms of discharge volume. The watershed area of the river is $\sim$ 230,000 km^2, which is mostly in the subtropical region with a long summer and a short winter. The total rainfall in the drainage basin is 1600–2000 mm yr^{-1}. Around 50% of the river runoff flows into the South China Sea (SCS) in summer between June and August (http://xxfb.hydroinfo.gov.cn/). During the past 30 yr, the Pearl River Delta has been affected by high loads of anthropogenic nutrients associated with the fast economic growth of China (Dai et al. 2006; Harrison et al. 2008). The average DIN concentration in the river end of the estuary is $\sim$ 100 μmol L^{-1} (Dai et al. 2008), which is somewhat intermediate when compared with other major river systems, such as the Rhine ($<$ 310 μmol L^{-1}), Mississippi ($\sim$ 128 μmol L^{-1}), and Amazon ($\sim$ 12 μmol L^{-1}) (van Bennekom and Wetsteijn 1990; DeMaster and Pope 1996; Rabouille et al. 2008).

The NSCS shelf stretches from the northwest to the southeast of mainland China with an area of about 1.2×10^6 km^2 (Fig. 1). In summer, coastal upwelling is driven by strong prevailing southwest monsoon winds over the nearshore NSCS due to Ekman pumping (Gan et al. 2009*a*) (shaded areas in Fig. 1) and interplays with the buoyant river plume caused by Pearl River flood (Gan et al. 2009*b*; Shu et al. 2011*a*). These two physical processes largely shape the nutrient dynamics and influence phytoplankton growth and the associated biological production (Gan et al. 2010; Cao et al. 2011).

Cruise background—Our cruise, based on the South China Sea Coastal Oceanographic Process Experiment (SCOPE) project, was conducted onboard the R/V *Shiyan III* from 29 June to 15 July 2008 (Fig. 1). The underway survey stations are shown in Fig. 1 marked as P3–P8 (on 29 June, in Leg 1) and U1–U9 (on 15 July, in Leg 2). Seven cross-shelf sections (named Transects 1–7) along the mapping survey covered the major plume-upwelling system in Leg 1 from 30 June to 08 July. During Leg 2 on 09–12 July, cross-shelf Transects 2–5 were repeatedly sampled. All stations were sited from the nearshore to the 300-m isobath except Transects 1 and 3 during Leg 1. Additional stations located between Transects 2 and 5 along the inner 30-m isobath are also shown in Fig. 1. Additional cruise information has also been introduced by Cao et al. (2011).

About 10 d prior to our cruise, continuous heavy rain peaked at $\sim$ 43,000 m^3 s^{-1} on 16 June but was down to $\sim$ 22,000 m^3 s^{-1} on 15 July (*see* fig. 2 in Cao et al. 2011). Such river discharges were much higher than the annual mean water discharge of about 6700 m^3 s^{-1}, or the monthly long-term average value of $\sim$ 14,000 m^3 s^{-1} in wet seasons from June to August (http://xxfb.hydroinfo.gov.cn/). As a result of the large water discharge from the Pearl River, the surface temperature in the entire Pearl River Estuary (PRE) had a narrow range of $\sim$ 26.7–28.7°C from the near null salinity zone to the estuary mouth and extending to the shelf area (Fig. 2). In contrast, salinity increased drastically from the upper estuary ($\sim$ 0.9–5.4) to the outer estuary (25.6–30.0) during both legs (Fig. 2).

The basic hydrology during the cruise over the NSCS shelf is presented in previous papers (Gan et al. 2009*a*,*b*; Cao et al. 2011). The study area is generally characterized by strong river plumes in the midshelf and upwelling nearshore. Patches of plume waters as manifested by warm temperature and low salinity (25.8–33.5) spread eastward over the shelf induced by abundant river discharge and altered by coastal upwelling circulation. During Leg 1, the river plume was extensive, extending $\sim$ 400 km away from the estuary mouth to the southern Taiwan Strait (Figs. 1, 2). In Leg 2, with the river discharge reduced and the ambient

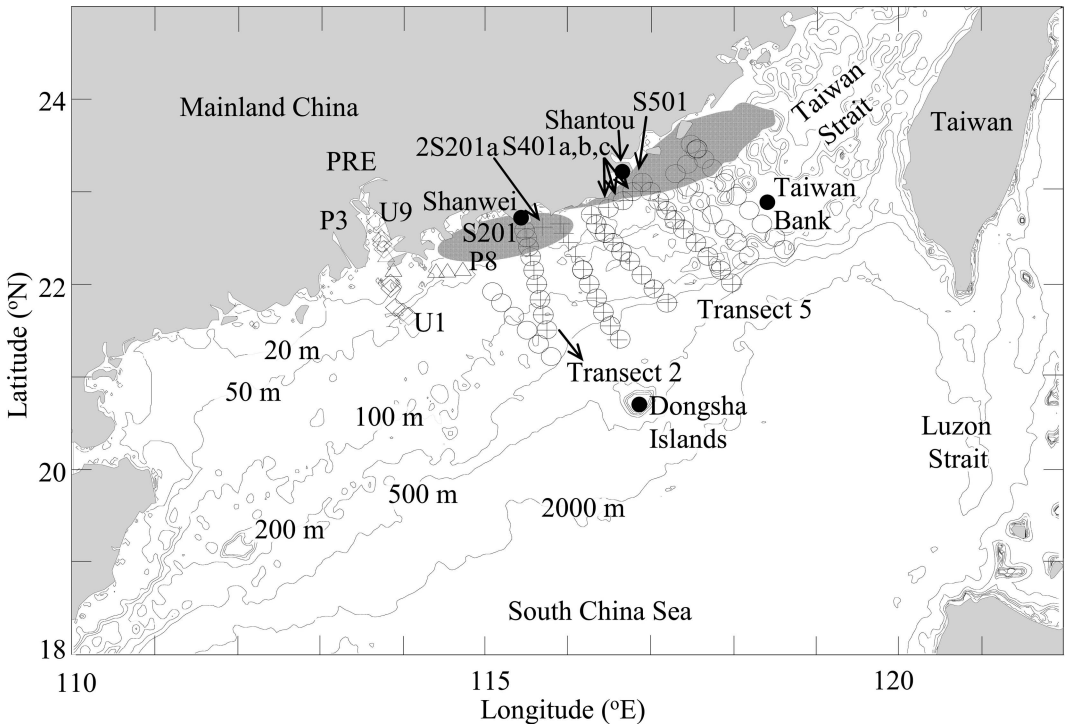

Fig. 1. Map of the northern South China Sea showing the cruise track, sampling transects, and topography. Shadowed areas indicate typical summer upwelling locations based on Gan et al. (2009*a*). The cruise included two legs: Transects 1–7 from 30 June to 08 July 2008 in Leg 1 (circles) and repeated Transects 2–5 surveyed from 09–12 July in Leg 2 (crosses). Also shown are underway sampling stations within the Pearl River Estuary (PRE), at Stas. P3–P8 (upper triangle) on 29 June and at Stas. U1–U9 (diamond) on 15 July. Additional stations located between Transects 2 and 3 (2S201a), and between Transects 4 and 5 (S401a–c, 2S401b–c) along the inner 30-m isobath are also displayed.

seawater being entrained into the plume water, salinity was elevated to 30.2–33.5 and the horizontal scale of low-salinity plume area (typical value < 29.0) shrank. Meanwhile, cold (22.8–26.0°C) and high-salinity (33.9–34.3) surface water appeared nearshore around 117°E during both legs, which were apparently induced by intensified coastal upwelling described by Gan et al. (2009*a*,*b*). In the outer shelf, offshore water with high temperature (27.3–28.7°C) and salinity (33.6–33.8) were horizontally homogeneous over the two legs.

Cross-shelf transects of temperature and salinity in Transect 2 during Legs 1 and 2 (Fig. 3) further displayed the bottom-hugging cold water tilted along the slope and toward the shore from > 100 m. The upwelling intensity appeared to be stronger during Leg 2, when cold (22.8–23.0°C) subsurface water outcropped at most nearshore stations. With regard to the Pearl River plume, during Leg 1, the plume water with salinity ranging from 25.8 to 33.5 flowed eastward and seaward over the diverging isobaths and was extended to ~ 50 km from the coast off Shanwei. Again in Leg 2, the plume water shrank with significantly elevated salinity ranging from ~ 28.2 to 33.5.

Farther east along Transect 5, the water was characterized by the warm and fresh river water in the upper layer and by cold and saline upwelled water nearshore in both legs with less influence by the plume in Leg 2 (Fig. 3). Shoreward extension of the river plume tended to inhibit the nearshore outcropping of the cold upwelled water, which originated upstream near Transect 2 where the narrowest shelf and strongest upslope cold water advection were located according to Gan et al. (2009*a*,*b*).

Sampling, analyses, and data processing—Nutrient samples were mainly collected in the shelf area from Niskin bottles mounted onto a Rosette sampling assembly, equipped with a conductivity–temperature–depth recorder (Sea-Bird SBE911). In addition, we collected several surface samples in the inner estuary (Stas. P3–P8 and U1–U9 in Fig. 1) using an underway pumping system similar to that described in Zhai et al. (2005). All nutrient samples were stored at −20°C until analysis.

Nutrient samples were run with a Technicon AA3 Auto-Analyzer (Bran-Lube, GmbH). DIN was analyzed using the copper–cadmium column reduction method as previously described (Dai et al. 2008), and DIP and $Si(OH)_4$ were measured using typical spectrophotometric methods (Knap et al. 1996). The linear working range we used was 0.1–17.6 μmol L^{-1} for DIN, 0.08–2.4 μmol L^{-1} for DIP, and 0.16–32 μmol L^{-1} for $Si(OH)_4$. The lower end of the concentration ranges represented the quantification limits. The detection limits for DIN, DIP, and $Si(OH)_4$ were 0.03 μmol L^{-1}, 0.03 μmol L^{-1}, and 0.05 μmol L^{-1}, respectively, and the analytical precision was better than 1% for DIN, 2% for DIP, and 2.8% for $Si(OH)_4$.

We also measured DIP at nmol L^{-1} levels according to Ma et al. (2008). Briefly, DIP was first extracted using a solid phase cartridge (Waters Oasis) by forming phosphomolybdenum blue, then eluted with sodium hydroxide

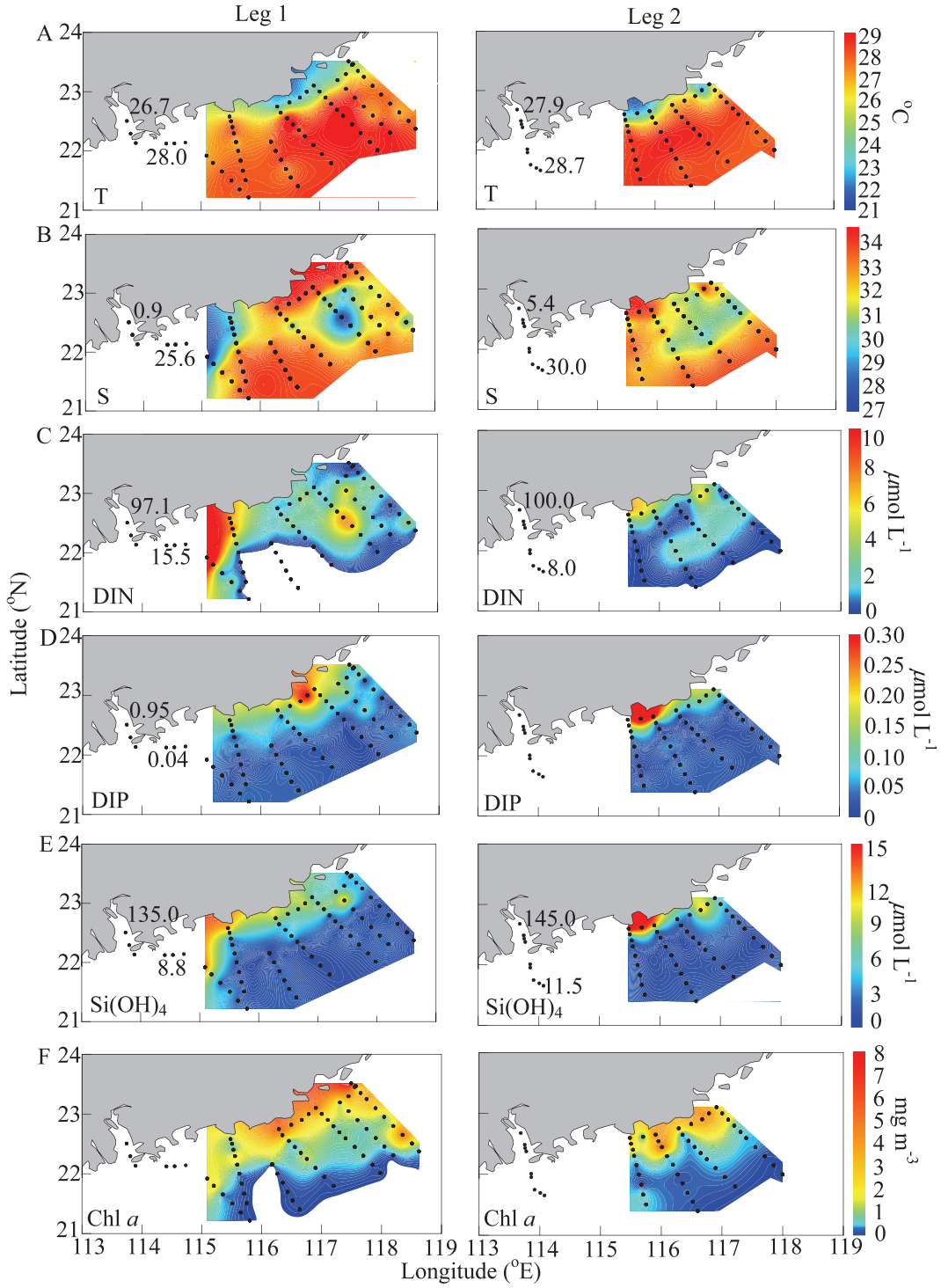

Fig. 2. Surface distribution (≤ 5 m) of (A) temperature (T, °C), (B) salinity (S), (C) dissolved inorganic nitrogen (DIN) (μmol L^{-1}), (D) dissolved inorganic phosphorus (DIP) (μmol L^{-1}), (E) silicate ($Si(OH)_4$) (μmol L^{-1}), and (F) chlorophyll *a* (Chl *a*) (mg m^{-3}) on the northern South China Sea shelf in summer 2008 during Legs 1 (left panels) and 2 (right panels). Also shown in numbers are values of the hydrochemical parameters at the river end member at near null salinity at Stas. P3 and U9 (black numerical value) and at the middle salinity area off the mouth of the Pearl River Estuary at Stas. P8, U1 (black numerical value).

solution. Flow injection analysis followed, and finally determination with a spectrophotometer. The detection limit for this method was 1.42 nmol L^{-1}, and the analysis precision was better than 5%. The working standard range adopted was 5–120 nmol L^{-1}, the lower end of which represented the quantification limit.

Samples for chlorophyll *a* (Chl *a*) analysis were filtered through 25-mm Whatman GF/F fiber filters and then were

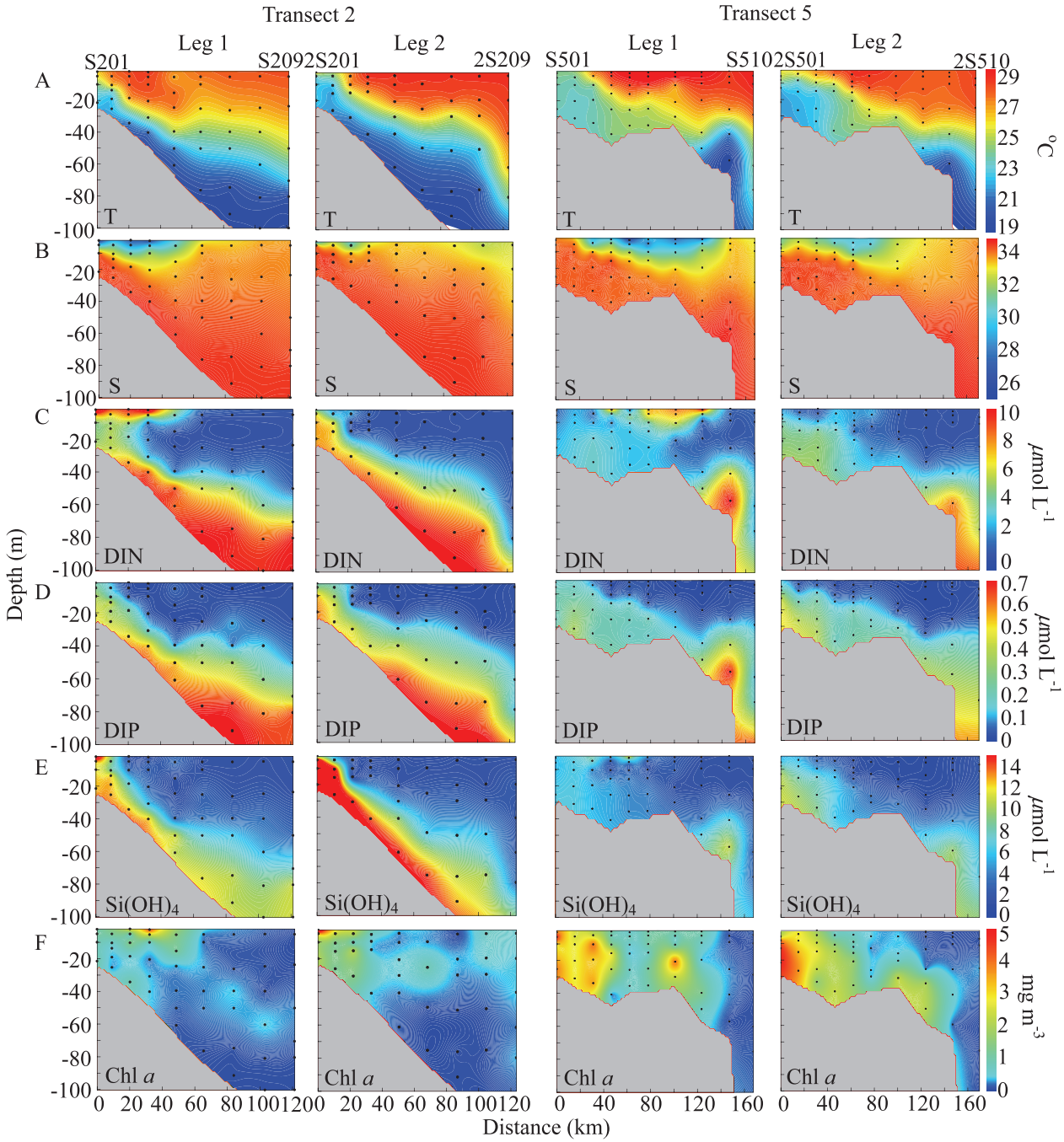

Fig. 3. Transectional distribution of T (°C), S, DIN (μmol L^{-1}), DIP (μmol L^{-1}), $Si(OH)_4$ (μmol L^{-1}), and Chl *a* (mg m^{-3}) in Transects 2 and 5 on the northern South China Sea shelf in summer 2008. The distributions of T and S in Transect 5 were redrawn from Shu et al. (2011*a*).

immediately frozen and stored in liquid nitrogen prior to analysis in the laboratory. These samples were later analyzed using a Turner fluorometer fitted with a red sensitive photomultiplier (Parsons et al. 1984).

Results

Surface distribution of nutrients—Surface nutrient concentrations from the underway stations (P3–P8 in Leg 1 and U1–U9 in Leg 2, Fig. 1) demonstrated a significant gradient inside the PRE. Moreover, the nutrient distribution along salinity gradients did not display a significant difference during the different sampling periods of Legs 1 and 2. For example, DIN ranged from ~ 100 μmol L^{-1} at near null salinity to ~ 8.0–15.5 μmol L^{-1} at the estuary mouth, and $Si(OH)_4$ decreased from ~ 135–145 μmol L^{-1} to ~ 8.8–11.5 μmol L^{-1} (Fig. 2). Meanwhile, DIP ranged from ~ 0.95 to ~ 0.04 μmol L^{-1} along the salinity gradient during Leg 1, decreasing significantly toward the estuary mouth (Fig. 2). Unfortunately, underway DIP values during Leg 2 were not available.

The hydrology of the NSCS shelf during our observation, as described above, was largely shaped by the plume in the midshelf and upwelling nearshore. As a consequence, distinguishable zonal nutrient patterns for the river plume and coastal upwelling were presented over the shelf (Fig. 2). Within the plume water, DIN concentrations were significantly elevated, mostly ranging from ~ 2.7 to 8.4 μmol L^{-1}. There were obvious differences in DIN concentration between the two legs, with < 0.1–14.2 μmol L^{-1} in Leg 1 and < 0.1–6.2 μmol L^{-1} in Leg 2. In contrast, DIP was relatively low at ~ 0.05 μmol L^{-1} ranging from ~ 0.02 to 0.30 μmol L^{-1} in Leg 1 and from ~ 0.02 to 0.30 μmol L^{-1} in Leg 2. $Si(OH)_4$ was ~ 1.5–3.8 μmol L^{-1}, being 0.2–18.9 μmol L^{-1} in Leg 1 and 0.9–11.7 μmol L^{-1} in Leg 2. In response to the abundant nutrients in the plume water, we observed enhanced phytoplankton biomass with Chl *a* values up to ~ 0.5–2.2 mg m^{-3} (Fig. 2). Nutrients around the upwelling area were also abundant. During Leg 1, the concentrations of DIN, DIP, and $Si(OH)_4$ in the upwelled waters off Shantou (Fig. 1) were 0.8–2.1 μmol L^{-1}, ~ 0.20 μmol L^{-1}, and 5.7–6.6 μmol L^{-1}, respectively; during Leg 2, coastal upwelling covered both Shantou and Shanwei with enhanced nutrient concentrations of ~ 3.5–6.4 μmol L^{-1} for DIN, ~ 0.25–0.37 μmol L^{-1} for DIP, and ~ 9.6–19.2 μmol L^{-1} for $Si(OH)_4$, suggesting the strengthening of the coastal upwelling intensity. In contrast, nutrients in the offshore surface water were < 0.1 μmol L^{-1} for DIN, ~ 0.02–0.03 μmol L^{-1} for DIP, and ~ 1.6–2.6 μmol L^{-1} for $Si(OH)_4$, indicating an overall oligotrophic condition.

Vertical distribution of nutrients—Vertical distribution of nutrients along Transects 2 and 5 during both sampling legs are shown in Fig. 3. DIN distribution was much like a composite of temperature and salinity, and the surface pattern generally followed the salinity distribution, as a result of upwelling circulation over the shelf (Gan et al. 2009*b*). In Transect 2, most values of DIN in the plume ranged from ~ 4.5 to 9.7 μmol L^{-1} in Leg 1, but were down to < 3.5 μmol L^{-1} in Leg 2 during the river discharge reduction phase, suggesting substantial nutrient consumption induced by phytoplankton growth. This was reflected by a maximum Chl *a* of 4.3 mg m^{-3} in Leg 1 and 6.6 mg m^{-3} in Leg 2 (Fig. 3). Similarly, $Si(OH)_4$ decreased from 0.7–18.9 μmol L^{-1} in Leg 1 to 1.4–6.7 μmol L^{-1} in Leg 2, further suggesting that the high biomass in the river plume was dominated by diatoms as revealed by a parallel study on phytoplankton composition (B. Q. Huang unpubl.). In contrast, DIP was at a quite stable level of ~ 0.02–0.22 μmol L^{-1} in both legs, which was also comparable to values in the outer shelf surface water (Fig. 3).

Underneath the buoyant plume water, there existed a strong onshore nutrient gradient owing to the bottom-hugging cold and nutrient-enriched water (DIN > 9.5 μmol L^{-1}, DIP > 0.65 μmol L^{-1}, and $Si(OH)_4$ > 10.3 μmol L^{-1}) from > 100 m deep along the Transact 2 slope (Fig. 3). Surface outcropping of DIN and $Si(OH)_4$ in the bottom boundary layer over the inner shelf in Leg 2 was likely attributable to the enhanced upwelling intensity. DIP values again displayed overall similarity during different sampling periods.

Owing to the eastward transport of the river plume, the plume center occupied the middle shelf of Transect 5 during Leg 1 and showed much lower DIN and $Si(OH)_4$ concentrations (2.5–8.4 μmol L^{-1} for DIN, 1.5–5.0 μmol L^{-1} for $Si(OH)_4$) than those in the plume center of Transect 2 in the same cruise period, suggesting nutrient consumption in the course of the plume water transport. Note that there was little difference in DIP between Transects 5 and 2 (Fig. 3). During Leg 2, DIN further declined to ~ 1.4–2.5 μmol L^{-1} and DIP and $Si(OH)_4$ decreased to the typical level of surface water over the outer SCS shelf area. In the intensified upwelling area off Shantou, nutrient concentrations (3.5–4.6 μmol L^{-1} for DIN, 0.30–0.49 μmol L^{-1} for DIP, and 5.9–10.7 μmol L^{-1} for $Si(OH)_4$) were markedly higher than those in Leg 1 (1.5–3.2 μmol L^{-1} for DIN, 0.16–0.31 μmol L^{-1} for DIP, and 4.1–6.7 μmol L^{-1} for $Si(OH)_4$) (Fig. 3).

Nutrient ratios in the water column—Nutrient ratios varied in conjunction with variations in nutrient concentrations. The areas predominated by plume waters during Leg 1 were characterized by high DIN : DIP (Fig. 4A) due to the "excess DIN" derived from the river input, whereas this high DIN : DIP ratio was not apparent as the river input was reduced in Leg 2 (Fig. 4A). Except in the plume water, the relationship between DIN and DIP (DIN : DIP) in the water column during the two legs was quite homogeneous with a slope of the linear regression line ~ 14.1 (Fig. 4A), conforming to the ratio in typical SCS subsurface water (Wong et al. 2007). With regard to $Si(OH)_4$: DIN in our plume-upwelling system, three characteristics appeared during the two legs (Fig. 4B): (1) the ratio of $Si(OH)_4$: DIN in subsurface water was generally close to the regression line, 1 : 1, and increased with depth, likely as a result of the slower biogenic silica dissolution or $Si(OH)_4$ regeneration from sinking particles as compared with the nitrogen regeneration (Koike et al. 2001); (2) lower $Si(OH)_4$: DIN ratio (< 1 : 1) in the plume regime, resulting from the higher diatom uptake. Indeed, diatom biomass was high in the plume region; and (3) as opposed to the plume regions, the $Si(OH)_4$: DIN ratio in the coastal upwelling was generally higher than 1 : 1. This may have been due to a combination of $Si(OH)_4$ uptake and addition (*see* discussion below).

Discussion

Derivation of the three end-member mixing model—Nutrient dynamics over the NSCS shelf in summer were largely modulated by biological uptake processes on top of the physical mixing. The potential temperature–salinity (θ–S) diagram illustrated a three end-member mixing scheme over the shelf (Fig. 5). In order to differentiate the solely physical mixing controlled nutrient distribution from the biological uptake in this plume-upwelling system, a three end-member mixing model was adopted as was used for the carbonate system in Cao et al. (2011), and only transects revisited (2–5) during Legs 1 and 2 were applied to the model for ease of comparison.

The mixing model is based on mass balance equations for potential temperature, salinity, and the water fractions

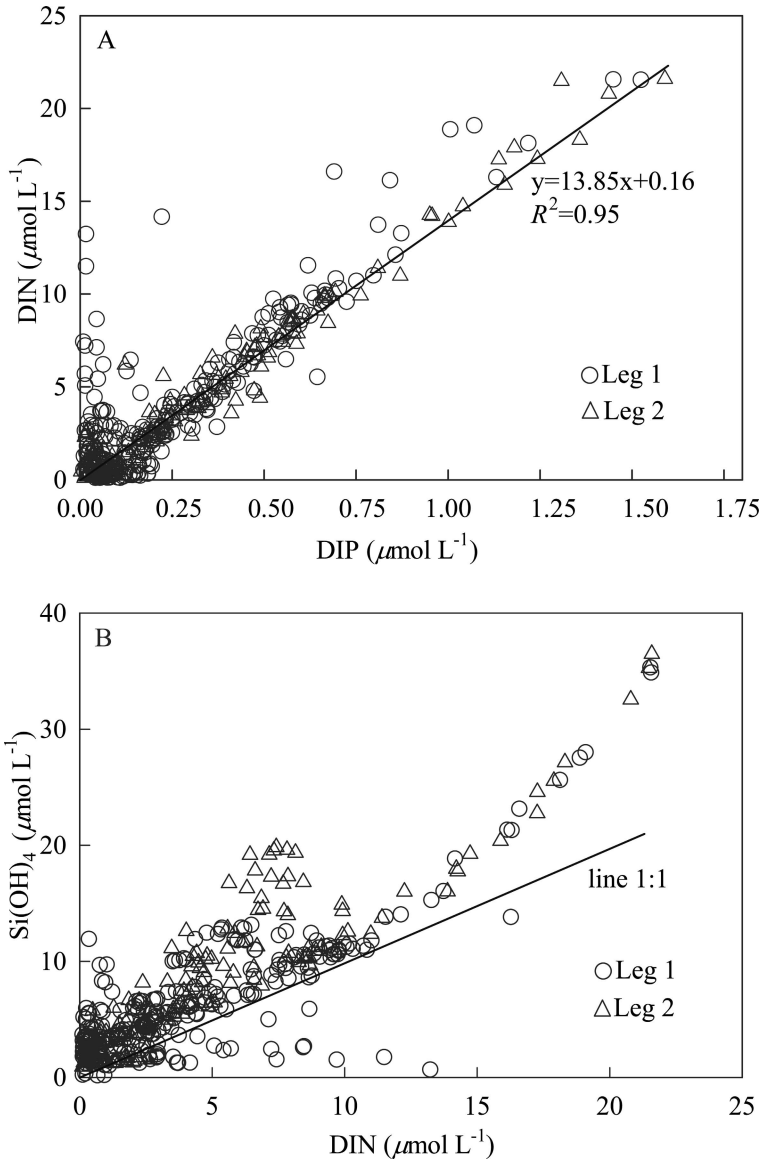

Fig. 4. (A) Correlation between DIN and DIP in the water column over the northern South China Sea shelf in summer 2008. The solid line denotes the regression curve between DIN and DIP in Leg 2 during the receding flood period. (B) Relationship between $Si(OH)_4$ and DIN in the water column. The solid line indicates the ratio of 1 : 1 for $Si(OH)_4$ vs. DIN.

originating from the three end members, as follows:

$$\theta_{RI}F_{RI}+\theta_{SW}F_{SW}+\theta_{SUB}F_{SUB}=\theta_{\text{in situ}} \quad (1)$$

$$S_{RI}F_{RI}+S_{SW}F_{SW}+S_{SUB}F_{SUB}=S_{\text{in situ}} \quad (2)$$

$$F_{RI}+F_{SW}+F_{SUB}=1 \quad (3)$$

where $\theta_{\text{in situ}}$ and $S_{\text{in situ}}$ represent the potential temperature and salinity in the samples; the subscripts *RI*, *SW*, and *SUB* denote the three different sources: Pearl River plume, the SCS surface water, and the subsurface water; and F_{RI}, F_{SW}, and F_{SUB} represent the fractions in the in situ water samples contributed by the three end members, which were calculated from the potential temperature and salinity.

The conservative nutrient concentrations of DIN (DIN°), DIP (DIP°), and $Si(OH)_4$ ($Si(OH)_4^\circ$) by mixing of the end members can then be calculated as

$$DIN^\circ=DIN_{RI}F_{RI}+DIN_{SW}F_{SW}+DIN_{SUB}F_{SUB} \quad (4)$$

$$DIP^\circ=DIP_{RI}F_{RI}+DIP_{SW}F_{SW}+DIP_{SUB}F_{SUB} \quad (5)$$

$$Si(OH)_4^\circ=Si(OH)_{4RI}F_{RI}+Si(OH)_{4SW}F_{SW}+Si(OH)_{4SUB}F_{SUB} \quad (6)$$

where DIN_{RI}, DIN_{SW}, DIN_{SUB}, DIP_{RI}, DIP_{SW}, DIP_{SUB}, $Si(OH)_{4RI}$, $Si(OH)_{4SW}$, and $Si(OH)_{4SUB}$ are the concentrations of the three end members for DIN, DIP, and $Si(OH)_4$.

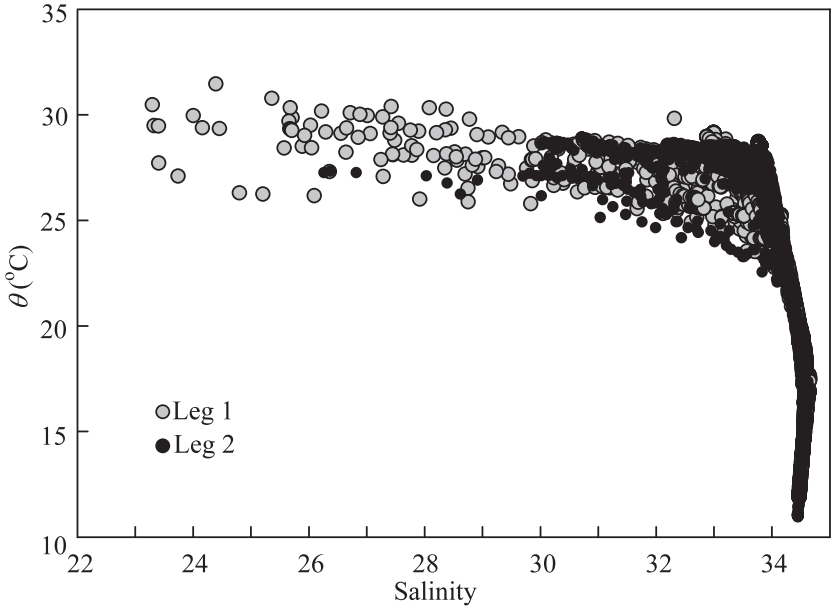

Fig. 5. The potential temperature (θ) (°C) vs. salinity scheme in the northern South China Sea collected from the conductivity–temperature–depth recorder per meter dataset in the whole water column involved in Legs 1 (Transects 1–7, shadow symbol) and 2 (Transects 2–5, solid symbol) (redrawn from Shu et al. 2011*b*). θ–S plots exhibit three water masses: river plume, SCS surface water, and SCS subsurface water.

The difference between the prediction based on conservative mixing and the field measured values was denoted as Δ, which reflected the amount of nutrients produced (negative) or removed (positive) associated with biological processes:

$$\Delta\mathrm{DIN} = \mathrm{DIN}^{\circ} - \mathrm{DIN}_{\text{in situ}} \tag{7}$$

$$\Delta\mathrm{DIP} = \mathrm{DIP}^{\circ} - \mathrm{DIP}_{\text{in situ}} \tag{8}$$

$$\Delta\mathrm{Si(OH)}_4 = \mathrm{Si(OH)}_4^{\circ} - \mathrm{Si(OH)}_{4\text{ in situ}} \tag{9}$$

where $\mathrm{DIN}_{\text{in situ}}$, $\mathrm{DIP}_{\text{in situ}}$, and $\mathrm{Si(OH)}_{4\text{ in situ}}$ represent the nutrient concentrations measured during the cruise.

The SCS surface water with $\theta \sim 28.6$°C and S ~ 33.7 served as the end member of the offshore surface water, and the colder SCS subsurface water with $\theta \sim 17.3$°C (in Leg 1) and ~ 16.8°C (in Leg 2) and S ~ 34.6 was defined as the end member of the subsurface water. We also defined the water with $\theta \sim 27$°C and S ~ 24.5 that tended to occupy the bulge off the PRE mouth (Gan et al. 2009*b*) to be the plume end member. The model parameters are presented in Table 1. From the above equations (Eqs. 7–9), uncertainty sources in the derivation of the delta terms are associated with the potential temperature, salinity, and the concentrations of nutrients of the end members. The composite uncertainty for average nutrient utilization values (ε) can be expressed as a function of θ_{RI}, θ_{SW}, θ_{SUB}, S_{RI}, S_{SW}, S_{SUB}, DIN_{RI}, DIN_{SW}, and DIN_{SUB}, i.e., $f(\theta_{RI}$, θ_{SW}, θ_{SUB}, S_{RI}, S_{SW}, S_{SUB}, DIN_{RI}, DIN_{SW}, and $\mathrm{DIN}_{SUB})$, based on the Taylor's expression (Taylor 1997):

$$\varepsilon_{\Delta\mathrm{DIN}} = \frac{1}{n} \times \sqrt{\sum_{i}^{n} \left(\begin{array}{l} \left(\frac{\partial(f)}{\partial([\theta_{RI}]_i)} \times \delta([\theta_{RI}]_i)\right)^2 + \left(\frac{\partial(f)}{\partial([\theta_{SW}]_i)} \times \delta([\theta_{SW}]_i)\right)^2 + \\ \left(\frac{\partial(f)}{\partial([\theta_{SUB}]_i)} \times \delta([\theta_{SUB}]_i)\right)^2 + \left(\frac{\partial(f)}{\partial([S_{RI}]_i)} \times \delta([S_{RI}]_i)\right)^2 + \\ \left(\frac{\partial(f)}{\partial([S_{SW}]_i)} \times \delta([S_{SW}]_i)\right)^2 + \left(\frac{\partial(f)}{\partial([S_{SUB}]_i)} \times \delta([S_{SUB}]_i)\right)^2 + \\ \left(\frac{\partial(f)}{\partial([\mathrm{DIN}_{RI}]_i)} \times \delta([\mathrm{DIN}_{RI}]_i)\right)^2 + \left(\frac{\partial(f)}{\partial([\mathrm{DIN}_{SW}]_i)} \times \delta([\mathrm{DIN}_{SW}]_i)\right)^2 + \\ \left(\frac{\partial(f)}{\partial([\mathrm{DIN}_{SUB}]_i)} \times \delta([\mathrm{DIN}_{SUB}]_i)\right)^2 \end{array} \right)} \tag{10}$$

where DIN is an example variable, δ_i is the uncertainty associated with potential temperature and salinity variation and the deviations range of nutrients in the plume end member, and n is the number of samples.

In our three end-member mixing model, we considered potential temperature to be conservative. This was under the condition that surface solar heating would not affect the conservativity of potential temperature, which could be argued however. It is known, on the other hand, that short wavelength solar radiation can only heat the very surface of the ocean, and thus the solar heating effect would be quite limited. This is evidenced by the fact that the sea surface temperature diurnal variation is on the order of ± 0.7°C in the NSCS basin (Dai et al. 2009). Note that such a diurnal change is reflective of an upper limit of surface solar heating effect, since wind may drive diapycnal mixing and thus the downward transport of heat to lower the temperature difference. Even if we assumed a potential temperature change of 1.0°C, the uncertainty introduced (Table 2) was much less than the relative standard deviation of average nutrient utilization values (spatial variabil-

Table 1. Summary of the end-member values adopted in our three end-member mixing model. Also shown are biological mediated nutrient variations denoted as ΔDIN, ΔDIP, and $\Delta Si(OH)_4$ (*see* text for details).

	θ (°C)	Salinity	DIN (μmol L^{-1})	DIP (μmol L^{-1})	$Si(OH)_4$ (μmol L^{-1})	ΔDIN (μmol L^{-1})	ΔDIP (μmol L^{-1})	ΔDIN : ΔDIP	$\Delta Si(OH)_4$ (μmol L^{-1})
Leg 1									
Plume*	27.0±1.0	24.5	30.0±5.0	0.30±0.05	36.0±4.0	4.2±2.7	0.08±0.05	52.5	5.5±4.3
Surface†	28.6±1.0	33.7±0.2	0.03±0.05	0.03±0.01	2.0±0.1				
Subsurface‡	17.3±1.0	34.6±0.05	12.9±2.0	0.91±0.19	15.6±5.0				
Coastal upwelling§						2.5±1.5	0.15±0.08	16.7	−0.4±2.3
Deep chlorophyll maximum						1.8±1.4	0.14±0.06	12.9	1.9±1.6
Leg 2									
Plume*	27.0±1.0	24.5	30.0±5.0	0.30±0.05	36.0±4.0	6.3±2.9	0.09±0.06	70.0	6.7±3.7
Surface†	28.6±1.0	33.7±0.2	0.03±0.05	0.03±0.01	2.0±0.1				
Subsurface‡	16.8±1.0	34.6±0.05	14.3±2.0	0.97±0.19	18.1±5.0				
Coastal upwelling§						2.0±1.3	0.12±0.09	16.7	−1.9±4.7
Deep chlorophyll maximum						2.3±1.0	0.14±0.06	16.4	1.0±2.2

* Plume water characterized by low salinity (< 33.5). Here, we defined the end member of plume water as $\theta \sim 27$°C and S ~ 24.5 that tended to occupy the bulge off the mouth of the Pearl River Estuary (Gan et al. 2009*b*).

† Surface water defined as sampling depth of ≤ 5 m and salinity of ~ 33.7. Average values of $\theta \sim 28.6$°C and S ~ 33.7 were used as the end member for this water type. Standard deviations from the averages are given after plus or minus signs. DIN concentration was according to Chen and Chen (2006).

‡ Subsurface water at the maximum salinity inflexion (S_{max}) in depth. The salinity maximum was 34.6, and the corresponding averages θ of 17.3°C in Leg 1 and 16.8°C in Leg 2 were defined as the end members for the water type.

§ Coastal upwelling was defined as the nearshore water with salinity > 33.75 in the upper 25 m.

ity, represented by ±) (Table 1). We therefore concluded that the solar heating effect would not influence our estimates of nutrient utilization rates.

Considering another conservative variable, salinity, we took the average salinity of 33.7 ± 0.2 as surface water end member, and the maximum salinity of 34.6 ± 0.05 as the subsurface water end member (Table 1). The uncertainty yielded by salinity was apparently related to the deviation values and, therefore, resulted in small variation in nutrient utilization values (Table 2). As for the plume water, no deviation was applied since a fixed salinity of 24.5 was adopted as its end member. As expected, the variation in nutrient utilization values induced by salinity turned out to be negligible, as shown in Table 2.

For the constraint of the nutrient end members, we observed that DIN remained overall conservative when salinity $< \sim 24.5$ but showed removal when S $> \sim 24.5$ during Leg 1 as shown in Fig. 6. During Leg 2 with the reduction of the river discharge, DIN was removed throughout the estuarine mixing. $Si(OH)_4$ had similar behavior to DIN along the salinity gradient. By contrast, there appeared to be a DIP excess likely induced by DIP addition or a buffer mechanism (Froelich 1988) involved in the midsalinity area at $\sim 10.0 <$ S $< \sim 24.5$, and a DIP deficit began when S was $> \sim 24.5$. Based on the above characteristics, we obtained average nutrient concentrations at S ~ 24.5, or at the plume bulge, to be ~ 30.0 μmol L^{-1} for DIN, ~ 0.30 μmol L^{-1} for DIP, and ~ 36.0 μmol L^{-1} for $Si(OH)_4$ assuming conservative mixing within the PRE (Fig. 6). Given the fact that the nutrient concentrations around null salinity during the two legs were rather constant, we considered the variations of nutrient concentrations of the plume end member to be ~ 5.0 μmol L^{-1} for DIN, ~ 0.05 μmol L^{-1} for DIP, and ~ 4.0 μmol L^{-1} for $Si(OH)_4$. These variations in the plume end members represented ~ 10–17% of the much higher average nutrient concentrations in the plume end member. The calculated uncertainties were much lower than the standard deviation of the average nutrient utilization values (Tables 1, 2). These points taken together, we contend that our results for nutrient utilization values were reasonable.

Nutrient consumption derived from the three end-member mixing model—The expected nutrient concentrations assuming simple dilution were derived from the three end-member mixing model (the triangular planes in Fig. 7). It was clear that most observational data were lower than the predicted values, representing a deficit due to biological uptake. Based on the difference between the predicted and measured values, we calculated the biological mediated nutrient variations in different water masses, which are summarized in Table 1.

Furthermore, the transectional distributions of biological mediated nutrient variations in Transect 2 are presented in Fig. 8 for further discussion. First, we see that most of ΔDIN and ΔDIP were positive and showed similar transectional patterns in both legs, suggesting DIN and DIP consumption during the upslope advection of the subsurface water from a depth ~ 100 m until it outcropped nearshore (Fig. 8A,B). Within this upwelling regime, ΔDIN

Table 2. Uncertainty (ε) assessment for the average nutrient utilization values in the three end-member mixing model during Legs 1 and 2. See Equation 10 for the uncertainty calculation. The variation of the variables used in the uncertainty estimation is listed in Table 1.

	$\varepsilon_{\Delta DIN}$ (μmol L^{-1})	$\varepsilon_{\Delta DIP}$ (μmol L^{-1})	$\varepsilon_{\Delta Si(OH)_4}$ (μmol L^{-1})	$\varepsilon_{\Delta DIN:\Delta DIP}$
Leg 1				
Plume	0.26	0.01	0.21	7.5
Coastal upwelling	0.22	0.02	0.43	2.5
Deep chlorophyll maximum	0.35	0.03	0.54	3.4
Leg 2				
Plume	0.24	0.01	0.21	8.1
Coastal upwelling	0.26	0.02	0.50	3.7
Deep chlorophyll maximum	0.57	0.03	0.69	5.8

values were averaged to $\sim 0.4 \pm 0.6$ μmol L^{-1} in Leg 1 and $\sim 0.9 \pm 0.5$ μmol L^{-1} in Leg 2 and ΔDIP were $\sim 0.07 \pm 0.03$ μmol L^{-1} in Leg 1 and $\sim 0.08 \pm 0.04$ μmol L^{-1} in Leg 2. In the upper layer ($\leq$ 25 m depth) of the coastal upwelling current alongshore with S > 33.75 from Shanwei to Shantou, or from Transects 2 to 5, average ΔDIN values during two legs were also at a similar level, with values of $\sim 2.5 \pm 1.5$ μmol L^{-1} in Leg 1 and $\sim 2.0 \pm 1.3$ μmol L^{-1} in Leg 2. The corresponding average ΔDIP values were 0.15 ± 0.08 μmol L^{-1} in Leg 1 and 0.12 ± 0.09 μmol L^{-1} in Leg 2, displaying again no obvious changes, although upwelling intensity appeared to be strengthened during Leg 2 (Fig. 9A,B). On the other hand, it should be noted that a few data points showed negative ΔDIN and ΔDIP along the coast (Fig. 9A,B), suggesting likely DIN and DIP additions sourced from organic matter degradation, and this is discussed below. Such regenerated DIN and DIP might have been consumed very quickly by phytoplankton

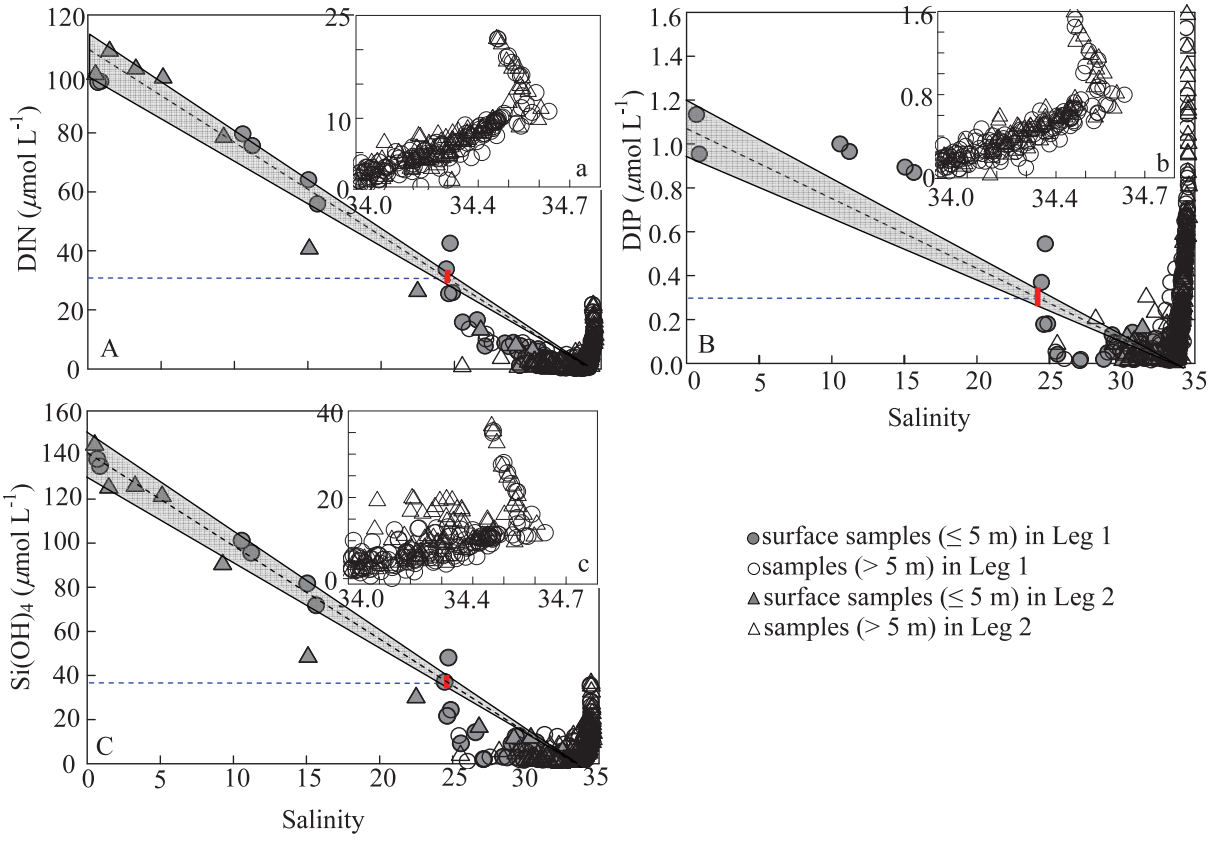

Fig. 6. Nutrient distributions along the salinity gradient (A) DIN; (B) DIP; (C) $Si(OH)_4$. The subsurface nutrient data at higher salinity (from 34.0–34.8) are also shown with expanded salinity scale (a) DIN; (b) DIP; (c) $Si(OH)_4$. The filled circles represent the surface data ($\leq$ 5 m) in Leg 1 including underway samples, and empty circles are subsurface water samples (> 5 m) in Leg 1, while the filled triangles denote the surface water samples ($\leq$ 5 m) in Leg 2 and the empty triangles are data from subsurface water samples (> 5 m) in Leg 2. The dashed line indicates the conservative mixing from the null salinity area to the saline water offshore. Shadowed areas represent the deviation amplitude of nutrient concentrations during conservative mixing, extrapolated from the variation of nutrient concentrations at null salinity. The blue dashed line represents the nutrient concentration on the conservative line at S $\sim$ 24.5, and the short red line denotes the deviation of nutrient concentrations at S $\sim$ 24.5.

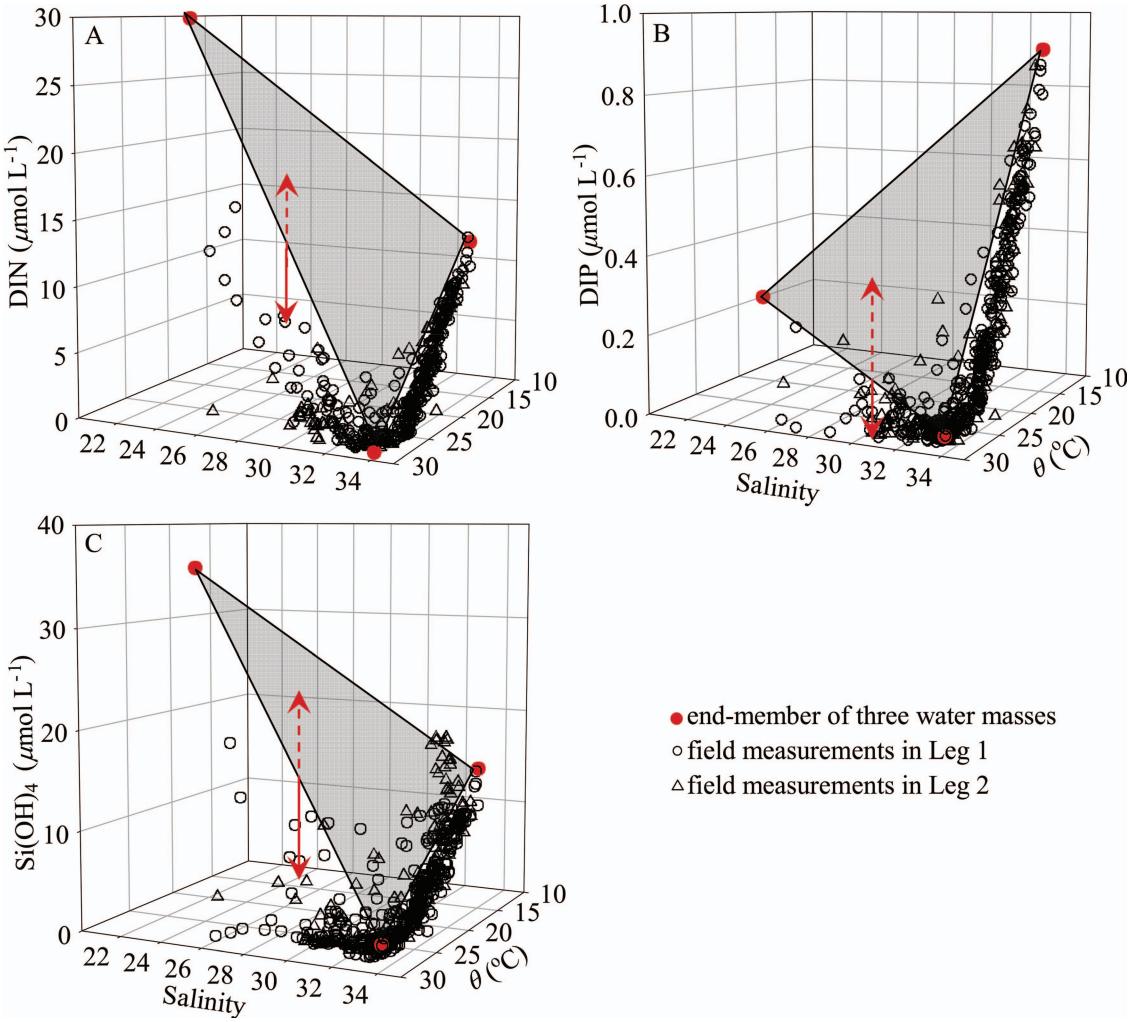

Fig. 7. Three-dimensional scatter relationships between θ (°C), salinity, and nutrients (A) DIN; (B) DIP; (C) $Si(OH)_4$. Note that the red dots represent the end members of the river plume (high T and low S), SCS surface water (high T and high S), and subsurface water (low T and high S). Shadowed panels represent the theoretical conservative nutrient distribution controlled solely by physical mixing processes. Black circles are data for nutrient concentrations from field measurement in Leg 1, while black triangles represent data in Leg 2. Red dashed arrows denote the difference of nutrient concentrations between the predicted conservative values and field measurements.

given the oligotrophic nature of the ambient water, the process of which, however, was difficult to elucidate.

As opposed to the mostly positive values of ΔDIN and ΔDIP along the northeastward coastal upwelling current from Shanwei to Shantou, most $\Delta Si(OH)_4$ values at Transect 2 around Shanwei were negative, ranging between ~ -4.6 and -2.6 μmol L^{-1} in Leg 1 and between ~ -10.0 and -6.1 μmol L^{-1} in Leg 2, suggesting that $Si(OH)_4$ addition occurred along the path of the upwelling circulation (Fig. 8C). However, along the northeastward coastal upwelling current, $\Delta Si(OH)_4$ became more and more positive. This is particularly true at the nearshore area of Transect 5 off Shantou, where the average values were 1.9 ± 1.0 μmol L^{-1} in Leg 1 and 1.4 ± 1.0 μmol L^{-1} in Leg 2 (Fig. 9C), suggesting northeastward enhancement of the biological consumption of $Si(OH)_4$.

The overall positive values in the river plume indicated net biological uptake (Fig. 8). Though the plume area was reduced during Leg 2 when the river discharge became weakened, the average ΔDIN displayed no great difference between the two legs, being 4.2 ± 2.7 μmol L^{-1} in Leg 1 and 6.3 ± 2.9 μmol L^{-1} in Leg 2 (Fig. 8A). The $\Delta Si(OH)_4$ distribution was similar to ΔDIN in the plume water column, with average values of 5.5 ± 4.3 μmol L^{-1} in Leg 1 and 6.7 ± 3.7 μmol L^{-1} in Leg 2 (Fig. 8C). However, ΔDIP values were extremely low at 0.08 ± 0.05 μmol L^{-1} in Leg 1 and 0.09 ± 0.06 μmol L^{-1} in Leg 2 (Fig. 8B; Table 1).

Nutrient uptake ratio, ΔDIN : ΔDIP, in the plume-upwelling system—Based on the model derived consumptions of individual nutrients, nutrient uptake ratios were estimated. The uptake ratios ΔDIN : ΔDIP in the coastal upwelling area were 16.7 in Leg 1 ($n > 35$) and 16.7 in Leg 2 ($n > 33$), conforming to the cellular Redfield ratio and the DIN : DIP ratio in the subsurface water column (Figs. 4A, 10). In contrast, the ΔDIN : ΔDIP values derived in the river plume were 52.5 ($n > 42$) in Leg 1 and 70.0 ($n > 47$) in Leg 2, greatly exceeding the classic Redfield stoichiometry (Fig. 10).

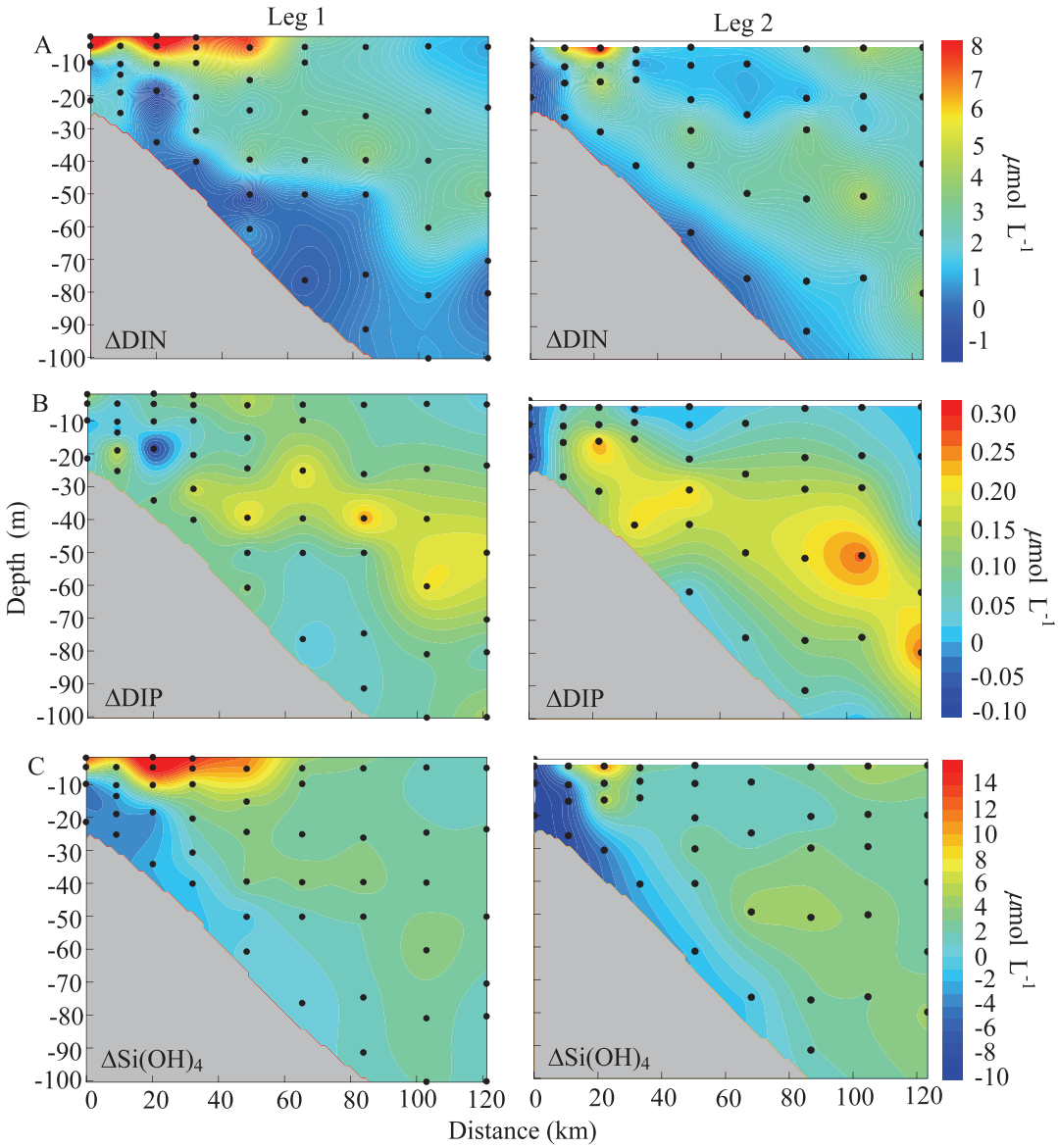

Fig. 8. Transectional distribution of (A) ΔDIN (μmol L^{-1}), (B) ΔDIP (μmol L^{-1}), and (C) $\Delta Si(OH)_4$ (μmol L^{-1}) in Transect 2 on the northern South China Sea shelf in summer 2008 during Leg 1 (left panels) and Leg 2 (right panels).

At the DCM layer located between ~ 20 and 60 m depths, the nutrient uptake was significantly enhanced, averaging 1.8 ± 1.4 μmol L^{-1} and 2.3 ± 1.0 μmol L^{-1} for ΔDIN, 0.14 ± 0.06 μmol L^{-1} and 0.14 ± 0.06 μmol L^{-1} for ΔDIP, and 1.9 ± 1.6 μmol L^{-1} and 1.0 ± 2.2 μmol L^{-1} for $\Delta Si(OH)_4$ during Legs 1 and 2, respectively (Fig. 8). Such distribution was consistent with the highest Chl *a* values (~ 0.5 mg m^{-3}) in the DCM layer (Fig. 3). Our derived ΔDIN : ΔDIP (12.9 for Leg 1 and 16.4 for Leg 2) at the DCM were also close to the Redfield ratio.

It is interesting to point out that although there was significant disturbance of physical settings, the levels of nutrient biological consumption in our cruise period were identical, lending additional evidence to our model derivation being generally in order. In addition, the consistent nutrient consumption regimes in between suggested that biological processes or biological metabolism tended to affect the nutrient composition for a longer duration when compared with physical processes as discussed in Zhai et al. (2009) based on the CO_2 partial pressure-dissolved oxygen relationship in the NSCS shelf region.

Redfield consumption in the coastal upwelling regimes—DIN : DIP uptake ratios in the coastal upwelling were identical to the Redfield ratio, and the nutrient consumption strongly stimulated phytoplankton productivity. As shown in Figs. 2, 3, average Chl *a* in the coastal upwelling ranged from 2.3 to 2.5 mg m^{-3} in both legs, and the maximum value was as high as 5.4 mg m^{-3}. Furthermore, production based on the ΔDIN in coastal upwelling was assessed to be 54 ± 24 mmol C m^{-2} d^{-1}, which was comparable to the primary production of 10–30 mmol C m^{-2} d^{-1} arrived at using numerical simulations (Gan et al. 2010) and to the net community production of 23 ± 26 mmol C m^{-2} d^{-1},

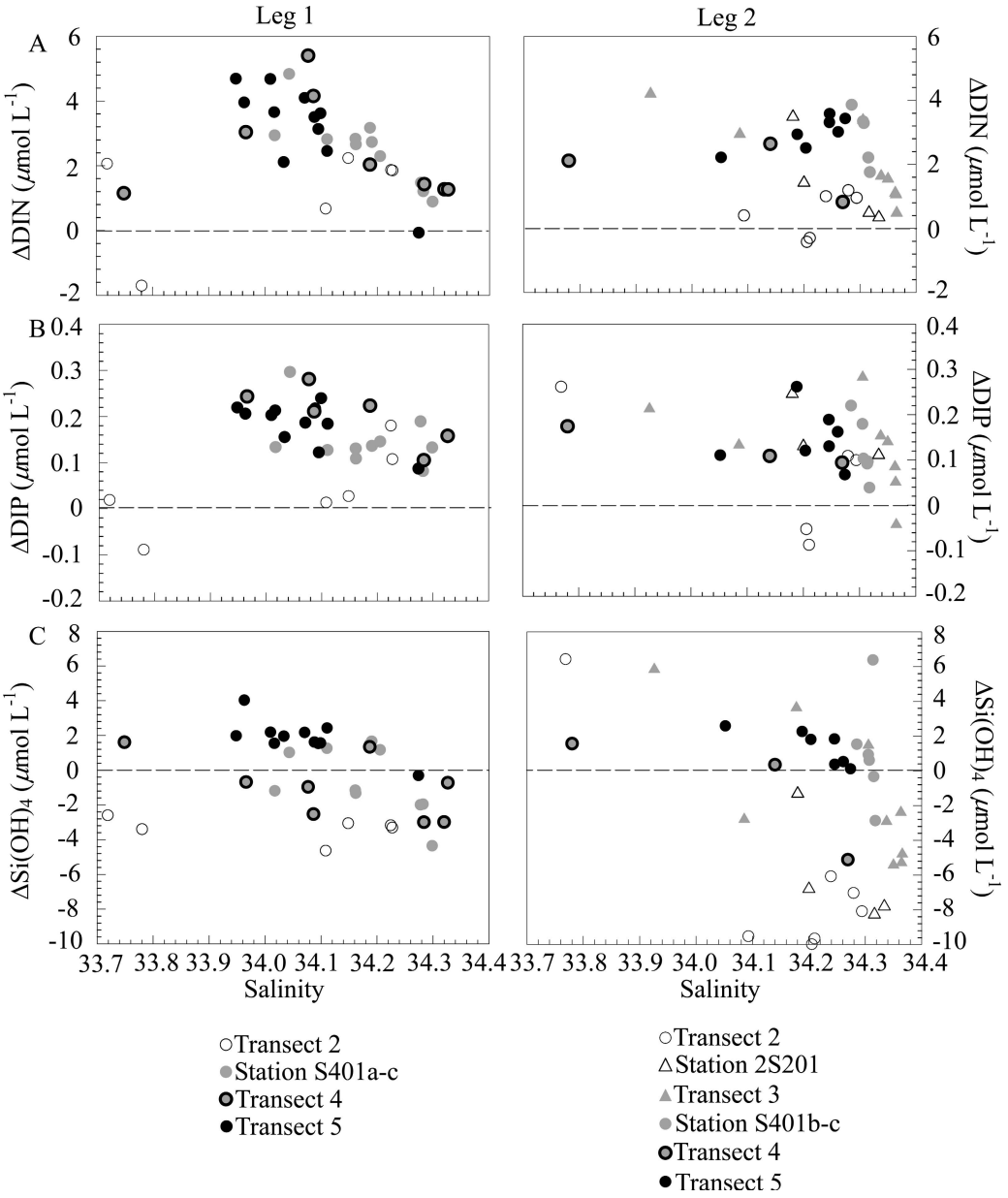

Fig. 9. Biological mediated nutrient variations vs. salinity in the coastal upwelling area from Transects 2 to 5 on the northern South China Sea shelf in summer 2008 during Leg 1(left panels) and Leg 2 (right panels). (A) ΔDIN (μmol L^{-1}), (B) ΔDIP (μmol L^{-1}), and (C) $\Delta Si(OH)_4$ (μmol L^{-1}).

dependent on the consumption of dissolved inorganic carbon (DIC) (Cao et al. 2011).

Apparent non-Redfield consumption in the plume regions—As discussed above, the most remarkable feature in these regions was the apparently high DIN : DIP uptake ratios, which significantly departed from the classic Redfield stoichiometry. Here, we cannot rule out the possibility of an alteration of the phytoplankton physiology leading to their different demand for DIN over DIP as reviewed by Arrigo (2005). Neither can we completely rule out the possibility of denitrification, which would remove DIN from the water column and thus lower the observed DIN : DIP ratios (Seitzinger and Giblin 1996). Nevertheless, we tended to believe that other nitrogen or phosphorus species or sources should have been adopted by the organisms to satisfy the Redfield ratio when the system was nutrient limited. Given the fact that other dissolved nitrogen sources such as dissolved organic nitrogen and urea could be ignored when compared with the abundant DIN concentration in the plume regime, we reasoned that DOP was the most probable non-DIP source to result in the apparently non-Redfield consumption ratios. Such reasoning can also be supported by the following two lines of evidence.

First, there have been a number of studies showing that P has a fast turnover rate supported by intracellular and

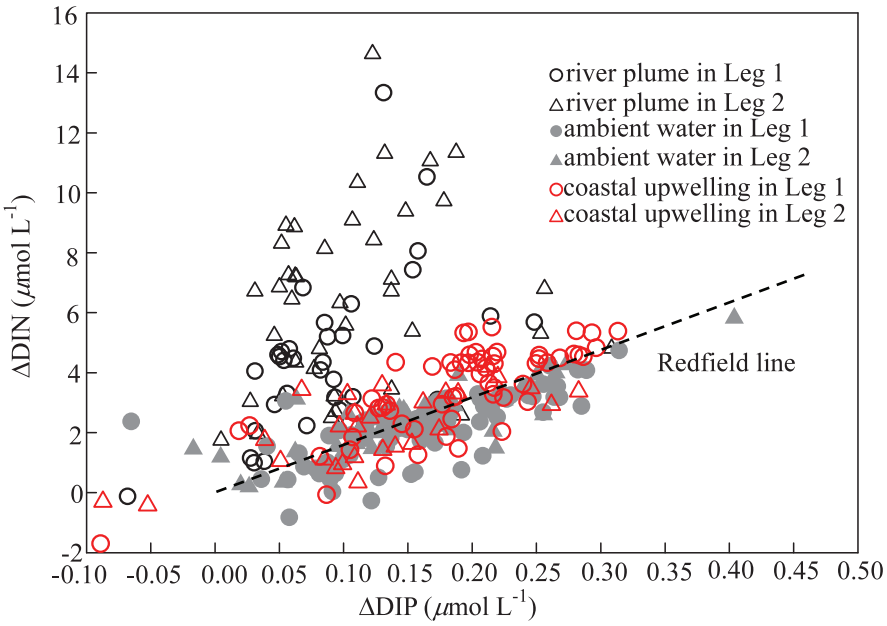

Fig. 10. Relationship between ΔDIN and ΔDIP in the water column from Transects 2 to 5 during Legs 1 and 2.

external DOP (Dyhrman et al. 2007) and P remineralization is preferential over that of N (Hopkinson et al. 2002). According to Dyhrman et al. (2007), the average turnover time of P within algal cells is only ~ 9 d when its concentration is ~ 40 nmol L^{-1}, and the turnover time tends to be even shorter when P becomes depleted (e.g., < 10 nmol L^{-1}). By contrast, the turnover time for N is much longer, e.g., 22–232 d according to Middelburg and Nieuwenhuize (2000). A rapid turnover rate of P may be very likely indicative of DOP production intracellularly and externally. The subsequent use of DOP in supporting phytoplanktonic metabolism is very often associated with elevated APA (Scanlan and Wilson 1999). In this study of plume waters, the average APA was ~ 212.5 ± 249.1 nmol L^{-1} h^{-1}, and the maximum was as high as ~ 972.8 nmol L^{-1} h^{-1} (B. Q. Huang unpubl.), confirming the great potential for DOP utilization.

Second, we performed a first order estimation of the DOP quantity required to meet the Redfield uptake assuming that the extra P was solely sourced from DOP. Such estimates would result in DOP concentrations of ~ 0.18 μmol L^{-1}–0.30 μmol L^{-1} for Legs 1 and 2. This predicted DOP concentration range matched well with the observed DOP concentration in prior studies in the lower PRE, which showed an average value of ~ 0.46 μmol L^{-1} (Lin et al. 2004).

Silicate dynamics in the plume-upwelling system—The negative $\Delta Si(OH)_4$ derived from our three end-member mixing model during the upslope advection at Transect 2 might have been due to net $Si(OH)_4$ input released from the sediments or suspended particles, a potential source term that could occur in the near-bottom water but was not accounted for in the mixing model. This is also explained by Álvarez-Salgado et al. (1997) and Cao et al. (2011). The general $\Delta Si(OH)_4$ increase along the northeastward coastal upwelling current from Transects 2 (negative) to 5 (positive) during both legs probably consisted of two components as confirmed by the DIC dynamics (Cao et al. 2011): net nutrient regeneration via organic matter degradation in the near-bottom onshore-flowing water and net nutrient uptake in the coastal upwelling current when outcropped and transported to the nearshore area, where organic matter production could occur. On the other hand, positive $\Delta Si(OH)_4$ in the river plume displayed a much higher level of ~ 5.5–6.7 μmol L^{-1}, indicating significant $Si(OH)_4$ consumption.

As shown above, in the coastal upwelling area off Shantou (Transect 5), $Si(OH)_4$ appeared to be predominantly consumed rather than regenerated. Based on the positive $\Delta Si(OH)_4$ and the information that the predominant group, the diatoms, were holding > 80% of the phytoplankton biomass (B. Q. Huang unpubl.), we were able to estimate the relative consumption ratios of $Si(OH)_4$: DIN, or $\Delta Si(OH)_4$: ΔDIN, of ~ 0.5–0.6, assuming the percentage abundance of diatoms was 100%. This derived uptake ratio was almost identical to the typical diatom elemental ratio of 0.65 (Brzezinski 1985; Kudo 2003; Lui and Chen 2011) and might contribute to the higher $Si(OH)_4$: DIN ratio in the coastal upwelling water column (Fig. 4B).

Meanwhile, since diatoms were ~ 50% in the plume (B. Q. Huang unpubl.), the $\Delta Si(OH)_4$: ΔDIN in this region was calculated to be 2.1–2.6, assuming that DIN is equally consumed by diatoms and nondiatoms. This higher $Si(OH)_4$: DIN uptake ratio could explain the $Si(OH)_4$: DIN variation along the Pearl River or Pearl River plume pathway, i.e., the ratio was > 1 : 1 at near null salinity ($Si(OH)_4$: DIN was ~ 140 μmol L^{-1} : 100 μmol L^{-1}, *see* Fig. 6) and was < 1 : 1 when extended over the shelf (Fig. 4B).

Taken together, we proposed a conceptual scheme of the nutrients dynamics coupled with that of DIC under the combined effects of the river plume and coastal upwelling (Fig. 11). During the intensified upslope and cross shelf

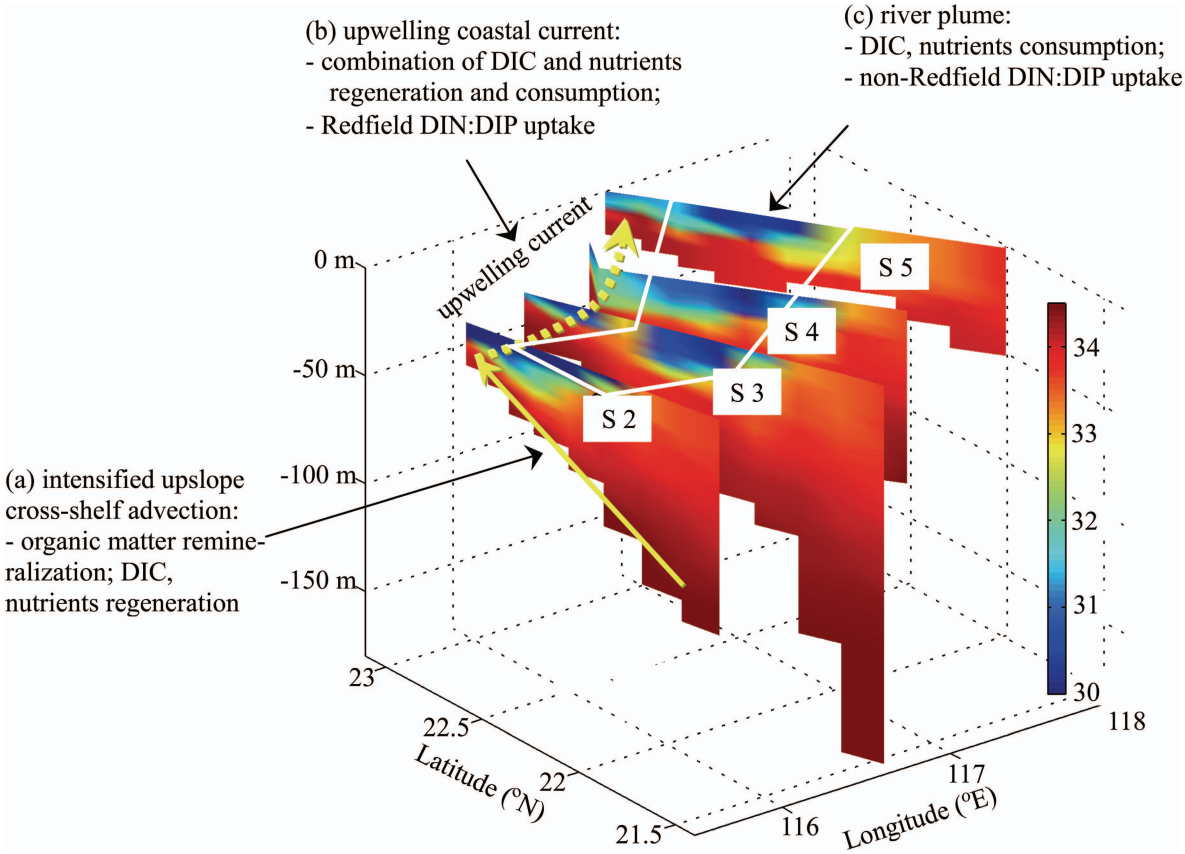

Fig. 11. Conceptual scheme illustrating nutrients (DIN, DIP, and $Si(OH)_4$) and dissolved inorganic carbon (DIC) dynamics under the co-influence of both the river plume and coastal upwelling over the northern South China Sea shelf. DIC dynamics was discussed in Cao et al. (2011), and the physical dynamics of the river plume and coastal upwelling was elucidated by Gan et al. (2009*a*,*b*). Basically, intensified upslope advection of subsurface waters that cross the middle shelf toward the inner shelf occurred near the head of a distinctly eastward widened shelf off Shanwei. The upwelled waters were subsequently transported northeastward by the upwelling coastal current and outcropped at the lee of the coastal cape off Shantou. Pearl River plume enhanced upwelling wind-driven current near surface while it was advected eastward. The salinity diagram was revised from Shu et al. (2011*a*). Symbols S2 to S5 represent the transect numbers 2 to 5. (a) Organic matter appeared to be remineralized, and DIC and nutrients were regenerated along with the upslope advection of subsurface waters toward Shanwei. (b) In the inner shelf along the upwelling coastal current from Shanwei to Shantou, there appeared a northward enhancement trend of DIC and nutrient consumption rates, although regeneration and consumption of DIC and nutrients (notably for $Si(OH)_4$) coexisted. DIN and DIP consumption followed the Redfield stoichiometry. (c) In the plume areas, net consumption of nutrients and DIC were obvious with an apparent non-Redfield DIN : DIP uptake ratio.

advection of subsurface waters toward Shanwei, remineralization of organic matter, or DIC and nutrients regeneration appeared to be dominant over nutrient or DIC consumption. In the inner shelf, along the upwelling current from Shanwei to Shantou, the consumption of DIC and nutrients, notably $Si(OH)_4$, was enhanced northeastwardly, although both regeneration and consumption existed. When the upwelled waters reached the lee of the coastal cape off Shantou, nutrient consumption became predominant. During the above upwelling circulation, the net DIN and DIP consumption followed the Redfield stoichiometry. In the plume areas, net consumption of nutrients and DIC were obvious with an apparent non-Redfield DIN : DIP uptake ratio.

We have addressed that high $\Delta DIN : \Delta DIP$ ratios in the plume system were related to the rapid turnover of P, thereby supplying non-DIP sources, or DOP, to satisfy the Redfield uptake. In this case, and if such a hypothesis stood, the non-DIP sources might have played equal or an even more important role in production within the river plume regime. Since the upwelled subsurface water primarily contained DIP, the non-DIP was unlikely to be sourced from upwelling. This might imply an underestimate of the often-used DIP proxy (Smith et al. 2010) for organic carbon production.

Acknowledgments

We thank Xiao Huang, Hua Lin, and Wentao He for their assistance in sample collection; the captain and the crew of R/V *Shiyan III* for their cooperation during the cruise; Dongxiao Wang, Jianyu Hu, and Qian Li for providing the conductivity–temperature–depth data and underway hydrographic data; and John Hodgkiss for assistance with English. This research was funded by the National Basic Research Program of China (973 Program) through grant 2009CB421204 and 2009CB421201, the National Natural Science Foundation of China through grants 90711005 and 40821063, and National Natural Science Foundation of China-Research Grants Council Hong Kong Special Administrative Region Government project (40731160624N and N_HKUST623/07). The sampling

cruise was supported by the South China Sea Coastal Oceano graphic Process Experiment project coorganized by Jiang Zhu, Dongxiao Wang, Xiaogang Guo, Minhan Dai, and Jianping Gan. Constructive comments from two anonymous reviewers and Dr. Robert R. Bidigare have greatly improved the quality of the paper.

References

Álvarez-Salgado, X. A., C. G. Castro, F. F. Pérez, and F. Fraga. 1997. Nutrient mineralization patterns in shelf waters of the Western Iberian upwelling. Cont. Shelf Res. **17:** 1247–1270, doi:10.1016/S0278-4343(97)00014-9

Arrigo, K. R. 2005. Marine microorganisms and global nutrient cycles. Nature **437:** 349–355, doi:10.1038/nature04159

Bianchi, T. S., and M. A. Allison. 2009. Large-river delta-front estuaries as natural 'recorders' of global environmental change. Proc. Natl. Acad. Sci. USA **106:** 8085–8092.

Brzezinski, M. A. 1985. The Si:C:N ratio of marine diatoms: Interspecific variability and the effect of some environmental variables. J. Phycol. **21:** 347–357, doi:10.1111/j.0022-3646.1985.00347.x

Cao, Z. M., M. H. Dai, N. Zheng, D. L. Wang, Q. Li, W. D. Zhai, F. F. Meng, and J. P. Gan. 2011. Dynamics of the carbonate system in a large continental shelf system under the influence of both a river plume and coastal upwelling. J. Geophys. Res. **116:** G02010, doi:10.1029/2010JG001596

Chen, C. T. A. 1996. The Kuroshio intermediate water is the major source of nutrients on the East China Sea continental shelf. Oceanol. Acta **19:** 523–527.

———. 2008. Buoyancy leads to high productivity of the Changjiang diluted water: A note. Acta Oceanol. Sin. **27:** 133–140.

———, K. K. Liu, and R. Macdonald. 2003. Continental margin exchanges, p. 82. *In* M. J. R. Fasham [ed.], Ocean biogeochemistry: The role of the ocean carbon cycle in global change. Springer-Verlag.

Chen, Y. L. L., and H. Y. Chen. 2006. Seasonal dynamics of primary and new production in the northern South China Sea: The significance of river discharge and nutrient advection. Deep-Sea Res. I **53:** 971–986, doi:10.1016/j.dsr.2006.02.005

Dagg, M. J., T. Bianchi, B. McKee, and R. Powell. 2008. Fates of dissolved and particulate materials from the Mississippi river immediately after discharge into the northern Gulf of Mexico, USA, during a period of low wind stress. Cont. Shelf Res. **28:** 1443–1450, doi:10.1016/j.csr.2006.12.009

Dai, M. H., X. H. Guo, W. D. Zhai, L. Y. Yuan, B. W. Wang, L. F. Wang, P. H. Cai, T. T. Tang, and W. J. Cai. 2006. Oxygen depletion in the upper reach of the Pearl River estuary during a winter drought. Mar Chem. **102:** 159–169, doi:10.1016/j.marchem.2005.09.020

———, Z. M. Lu, W. D. Zhai, B. S. Chen, Z. M. Cao, K. B. Zhou, W. J. Cai, and C. T. A. Chen. 2009. Diurnal variations of surface seawater pCO_2 in contrasting coastal environments. Limnol. Oceanogr. **54:** 735–745, doi:10.4319/lo.2009.54.3.0735

———, L. F. Wang, X. H. Guo, W. D. Zhai, Q. Li, B. Y. He, and S. J. Kao. 2008. Nitrification and inorganic nitrogen distribution in a large perturbed river/estuarine system: The Pearl River Estuary, China. Biogeosciences **5:** 1227–1244, doi:10.5194/bg-5-1227-2008

DeMaster, D. J., and R. H. Pope. 1996. Nutrient dynamics in Amazon shelf waters: Results from AMASSEDS. Cont. Shelf Res. **16:** 263–289, doi:10.1016/0278-4343(95)00008-O

Dyhrman, S. T., J. W. Ammerman, and B. A. S. V. Mooy. 2007. Microbes and the marine phosphorus cycle. Oceanography **20:** 110–116, doi:10.5670/oceanog.2007.54

Froelich, P. N. 1988. Kinetic control of dissolved phosphate in natural rivers and estuaries: A primer on the phosphate buffer mechanism. Limnol. Oceanogr. **33:** 649–668, doi:10.4319/lo.1988.33.4_part_2.0649

Gan, J. P., A. Cheung, X. G. Guo, and L. Li. 2009*a*. Intensified upwelling over a widened shelf in the northeastern South China Sea. J. Geophys. Res. **114:** C09019, doi:10.1029/2007JC004660

———, L. Li, D. X. Wang, and X. G. Guo. 2009*b*. Interaction of a river plume with coastal upwelling in the northeastern South China Sea. Cont. Shelf Res. **29:** 728–740, doi:10.1016/j.csr.2008.12.002

———, Z. M. Lu, M. H. Dai, A. Y. Y. Cheung, H. B. Liu, and P. Harrison. 2010. Biological response to intensified upwelling and to a river plume in the northeastern South China Sea: A modeling study. J. Geophys. Res. **115:** C09001, doi:10.1029/2009JC005569

Geider, R. J., and J. L. Roche. 2002. Redfield revisited: Variability of C:N:P in marine microalgae and its biochemical basis, European. J. Phycol. **37:** 1–17, doi:10.1017/S0967026201003456

Harrison, P. J., K. D. Yin, J. H. W. Lee, J. P. Gan, and H. B. Liu. 2008. Physical-biological coupling in the Pearl River estuary. Cont. Shelf Res. **28:** 1405–1415, doi:10.1016/j.csr.2007.02.011

Hopkinson, C. S., J. J. Vallino, and A. Nolin. 2002. Decomposition of dissolved organic matter from the continental margin. Deep-Sea Res. II **49:** 4461–4478, doi:10.1016/S0967-0645(02)00125-X

Jickells, T. D. 1998. Nutrient biogeochemistry of the coastal zone. Science **281:** 217–222, doi:10.1126/science.281.5374.217

Karl, D. M., and K. M. Björkman. 2002. Dynamics of DOP, p. 249–366. *In* D. A. Hansell and C. A. Carlson [eds.], Biogeochemistry of marine dissolved organic matter. Elsevier Science.

Knap, A., A. Michaels, A. Close, H. Ducklow, and A. Dickson. 1996. Protocols for the Joint Global Ocean Flux Study (JGOFS) Core Measurements, p. 43–90. JGOFS Report No. 19, vi + 170 pp. Reprint of the IOC Manuals and Guides No. 29, UNESCO 1994.

Koike, I., H. Ogawa, T. Nagata, R. Fukuda, and H. Fukuda. 2001. Silicate to nitrogen ratio of the upper Sub-Arctic Pacific and the Bering Sea Basin in summer: Its implication for phytoplankton dynamics. J. Oceanogr. **57:** 253–260, doi:10.1023/A:1012474327158

Kudo, I. 2003. Change in the uptake and cellular Si:N ratio in diatoms responding to the ambient Si:N ratio and growth phase. Mar. Biol. **143:** 39–46, doi:10.1007/s00227-003-1063-2

Lin, Y. A., J. L. Su, C. Y. Hu, M. Zhang, Y. Li, W. B. Guan, and J. C. Chen. 2004. N and P in waters of the Zhujiang River Estuary in summer. Acta Oceanol. Sin. **26:** 63–73. [In Chinese]

Lohrenz, S. E., G. L. Fahnenstiel, D. G. Redalje, G. A. Lang, M. J. Dagg, T. E. Whitledge, and Q. Dortch. 1999. Nutrients, irradiance, and mixing as factors regulating primary production in coastal waters impacted by the Mississippi River plume. Cont. Shelf Res. **19:** 1113–1141, doi:10.1016/S0278-4343(99)00012-6

Lui, H. K., and C. T. A. Chen. 2011. Shifts in limiting nutrients in an estuary caused by mixing and biological activity. Limnol. Oceanogr. **56:** 989–998, doi:10.4319/lo.2011.56.3.0989

Ma, J., D. X. Yuan, and Y. Liang. 2008. Sequential injection analysis of nanomolar soluble reactive phosphorus in seawater with HLB solid phase extraction. Mar. Chem. **111:** 151–159, doi:10.1016/j.marchem.2008.04.011

Middelburg, J. J., and J. Nieuwenhuize. 2000. Nitrogen uptake by heterotrophic bacteria and phytoplankton in the nitrate-rich Thames estuary. Mar. Ecol. Prog. Ser. **203:** 13–21, doi:10.3354/meps203013

Nicholson, D., S. Dyhrman, and A. Paytan. 2006. Alkaline phosphatase activity in the phytoplankton communities of Monterey Bay and San Francisco Bay. Limnol Oceanogr. **51:** 874–883, doi:10.4319/lo.2006.51.2.0874

Parsons, T. R., Y. Maita, and C. M. Lalli. 1984. A manual of chemical and biological methods for seawater analysis. Pergamon.

Rabouille, C., and others. 2008. Comparison of hypoxia among four river-dominated ocean margins: The Changjiang (Yangtze), Mississippi, Pearl, and Rhône rivers. Cont. Shelf Res. **28:** 1527–1537, doi:10.1016/j.csr.2008.01.020

Redfield, A. C., B. H. Ketchum, and F. A. Richards. 1963. The influence of organisms on the composition of seawater, p. 26–77. *In* M. N. Hill [ed.], The composition of seawater. Comparative and descriptive oceanography. The sea, volume 2: Ideas and observations on progress in the study of the seas. Interscience Publishers.

Scanlan, D. J., and W. H. Wilson. 1999. Application of molecular techniques to addressing the role of P as a key effector in marine ecosystems. Hydrobiologia **401:** 149–175, doi:10.1023/A:1003742528262

Seitzinger, S. P., and A. E. Giblin. 1996. Estimating denitrification in North Atlantic continental shelf sediments. Biogeochemistry **35:** 235–260, doi:10.1007/BF02179829

Shu, Y. Q., D. X. Wang, J. Zhu, and S. Q. Peng. 2011*a*. The 4-D structure of upwelling and Pearl River plume in the northern South China Sea during summer 2008 revealed by a data assimilation model. Ocean Model. **36:** 228–241, doi:10.1016/j.ocemod.2011.01.002

———, J. Zhu, D. X. Wang, and X. J. Xiao. 2011*b*. Assimilating remote sensing and in situ observations into a coastal model of northern South China Sea using ensemble Kalman filter. Cont. Shelf Res. **31:** S24–S36, doi:10.1016/j.csr.2011.01.017

Smith, S. V., D. P. Swaney, and L. Talaue-McManus. 2010. Carbon-nitrogen-phosphorus fluxes in the Coastal Zone: The LOICZ approach to global assessment, p. 575–577. *In* K. K. Liu, L. Atkinson, R. Quiñones, and L. Talaue-McManus [eds.], Carbon and nutrient fluxes in continental margins. Springer-Verlag.

Taylor, J. R. 1997. An introduction to error analysis, 2nd ed. University Science Books.

van Bennekom, A. J., and F. J. Wetsteijn. 1990. The winter distribution of nutrients in the Southern Bight of the North Sea (1961–1978) and in the estuaries of the Scheldt and the Rhine/Meuse. Neth. J. Sea Res. **25:** 75–87, doi:10.1016/0077-7579(90)90010-E

van Geen, A., R. K. Takesue, J. Goddard, T. Takahashi, J. A. Barth, and R. L. Smith. 2000. Carbon and nutrient dynamics during coastal upwelling off Cape Blanco, Oregon. Deep-Sea Res. II **47:** 975–1002, doi:10.1016/S0967-0645(99)00133-2

Varkitzi, I., K. Pagou, E. Granéli, I. Hatzianestis, C. Pyrgaki, A. Pavlidou, B. Montesanto, and A. Economou-Amilli. 2010. Unbalanced N:P ratio and nutrient stress controlling growth and toxin production of the harmful dinoflagellate *Prorocentrum lima* (Ehrenberg) Dodge. Harmful Algae **9:** 304–311, doi:10.1016/j.hal.2009.12.001

Wong, G. T. F., C. M. Tseng, L. S. Wen, and S. W. Chung. 2007. Nutrient dynamics and N-anomaly at the SEATS station. Deep-Sea Res. II **54:** 1528–1545, doi:10.1016/j.dsr2.2007.05.011

Zhai, W. D., M. D. Dai, and W. J. Cai. 2009. Coupling of surface pCO_2 and dissolved oxygen in the northern South China Sea: Impacts of contrasting coastal processes. Biogeosciences **6:** 2589–2598, doi:10.5194/bg-6-2589-2009

———, ———, ———, Y. C. Wang, and Z. H. Wang. 2005. High partial pressure of CO_2 and its maintaining mechanism in a subtropical estuary: The Pearl River estuary. China. Mar. Chem. **93:** 21–32.

Associate editor: Robert R. Bidigare

Received: 18 June 2011
Accepted: 09 November 2011
Amended: 16 December 2011